# INFLUENCE OF DIFFERENT WIND ANGLES ON PEDESTRIAN WIND COMFORT IN 3D SPACE

N. Ridzuan[1*], U. Ujang[1], S. Azri[1] , T. L. Choon[2]

[1] 3D GIS Research Lab, Faculty of Built Environment and Surveying, Universiti Teknologi Malaysia, Johor, Malaysia
[2] Geoinformation, Faculty of Built Environment & Surveying, Universiti Teknologi Malaysia, Johor, Malaysia
(nurfairunnajiha2@graduate.utm.my, (mduznir, suhaibah & tlchoon)@utm.my)

**KEY WORDS:** Pedestrian Wind Comfort, Computational Fluid Dynamics, Wind Simulation, Roof Overhang, CityGML.

**ABSTRACT:**

Wind can impact pedestrian comfort. This comfort can be observed by integrating a 3D city model into the study area. However, little research has been done on the influence of different wind angles on pedestrian wind comfort and rarely on implementing 3D city models in the wind environment. Therefore, this study aims to fill the gap in using 3D city models to examine the effect of wind flow angles on pedestrian wind comfort. The Computational Fluid Dynamics (CFD) wind simulation environment presented in this study was constructed through the applied steady Reynolds-Average Navier-Stokes (RANS) with K-epsilon (k-ε) turbulence model. It is integrated with the standalone building model with a roof overhang structure represented in LoD2.3 of the CityGML standard. Three wind angles have been introduced to allow for variation in the analysis of pedestrian wind comfort: 0˚, 15˚, and 30˚ wind angles. Through the observation of multiple locations, which are directed beneath the roof overhang structure, the highest wind velocity is recorded in 0˚ wind angles compared to 15˚ and 30˚ wind angles. Thus, from these recorded values, pedestrian wind comfort is based on the Beaufort wind scale (BWS). The computed average recorded values show that 3.24 m/s corresponds to a wind angle of 0°, 2.761 m/s for 15˚, and 2.415 m/s for 30˚, which shows that all these values fall in BWS Scale 2. Thus, these areas experience a light breeze. However, the lowest value from a 30-degree environment presents the most reposeful surrounding.

## 1. INTRODUCTION

The impact of wind on pedestrian comfort has been an ongoing research topic in urban design and planning. The study of wind flow patterns and their influence on pedestrian wind comfort is critical in creating liveable urban environments. The use of 3D city models has been instrumental in analysing urban microclimates and understanding the wind patterns that affect pedestrian comfort. Recent studies have used 3D city models to study urban heat islands, heritage house maintenance, and visualising urban air quality, providing useful information for urban planners and designers (Azri et al., 2018; Mohd et al., 2017; Ridzuan et al., 2020; Salleh et al., 2021; Ujang et al., 2018).

However, little research has been done on the influence of different wind angles on pedestrian wind comfort. This article seeks to address this research gap by using 3D city models to investigate the impact of wind flow angles on pedestrian wind comfort. By analysing the patterns of wind flow and their influence on pedestrian comfort from different angles, this study can provide valuable information for urban planners and designers to create comfortable pedestrian environments. This study can contribute to the 3D data structure for the implementation of geomarketing strategies, known as Voronoi classified and clustered data constellation, which can be used for future study of urban microclimates and wind flow patterns (Azri et al., 2020; Ujang et al., 2013).

Wind flow pattern change along with the presented shape and design of the building model. Wind simulation of the CFD technique is a commonly performed approach to observe the ambient wind. However, research in this field seldom utilised standardized building models; instead, several researchers, such as García-Sánchez et al. (2021); Ridzuan & Ujang (2021), use 3D city modelling with the CityGML standard to represent the building model. This study continues to implement the modelling standard to provide a suitable detailing and complexity of the building model based on the level of detail concept. One of the structures, such as a roof overhang, can be included in the building model. In addition to that, the angle of incidence of the incoming wind is various, which can further manipulate the wind flow. Therefore, this study used the building model with this structure to observe its impact on the wind simulation outcome from different wind directions. Furthermore, the wind simulation process can assist in determining pedestrian wind comfort (Hågbo et al., 2021). Therefore, from the resulting simulation, the level of study presents the wind comfort to show the influence of the different wind angles on pedestrian wind comfort. Through this research, we hope to improve the understanding of the impact of wind flow angles on pedestrian wind comfort and provide information for the design of comfortable urban environments.

## 2. METHODOLOGY

To perform this study, three phases are required: acquisition and modelling, simulation, and analysis (Figure 2).

### 2.1 Data Acquisition and Modelling

The building model used in this study is based on the Level of Detail (LoD) concept, specifically LoD2.3, which includes the roof overhang structure. This building model is the regeneration of a real-world building. However, the model has been simplified into the LoD2.3 building model. Furthermore, the existing structure of the roof overhang on the model becomes the reason for choosing this model. This is due to this structure's ability to allow for air movement below the building structure and its ability to influence the wind simulation outcomes. Figure 1 shows the utilized standalone building model used in this study.

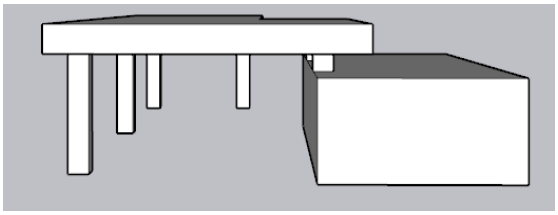

**Figure 1**. 3D building model of LoD2.3.

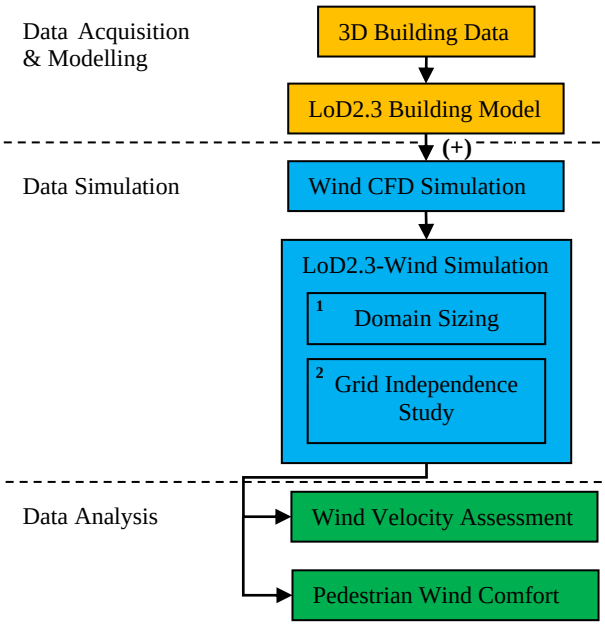


**Figure 2.** Workflow for a single-degree wind angle.

### 2.2 Data Simulation

The simulation phase involves running a wind Computational Fluid Dynamics (CFD) simulation using an embedded building model with the roof overhang structure. Three CFD environments must be constructed as there are three different wind directions, 0˚, 15˚, and 30˚, to be observed. The simulation domain is constructed following the domain size approach of Franke et al. (2007), with dimensions of the upstream ($l_u$) and lateral sides (b), the downstream side ($l_d$), and domain height of 5H, 15H, and 6H (40.32m), respectively, where H is the height of the building = 6.72m (Figure 3).

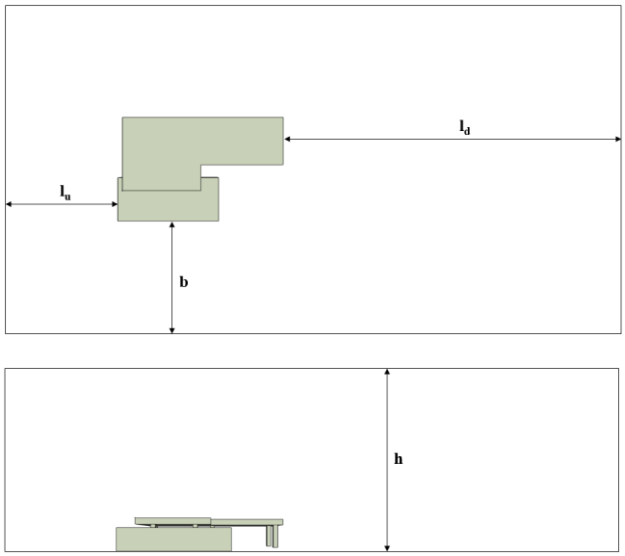


**Figure 3**. Wind simulation domain, $l_u$ = 33.6m, b = 33.6m, $l_d$ = 114.22m and h = 40.32m.

In addition, the steady Reynolds-Average Navier-Stokes (RANS) with K-epsilon (k-ε) turbulence model is implemented for all three environments to support the wind computation (Singh & Roy, 2019). This simulation is known as incompressible wind flow. The Navier-Stokes equations are coupled with Reynolds decomposition to create this RANS equation, and the parameter values are separated into a sum of the mean and fluctuating components. The equations are as follows:

$$\frac{\partial \bar{u}_i}{\partial x_i} = 0 \tag{1}$$

$$\frac{\partial \bar{u}_i}{\partial t} + \frac{\partial}{\partial x_j}\left(\bar{u}_i\,\bar{u}_j\right) = -\frac{1}{\rho}\frac{\partial \bar{p}}{\partial x_i} + \frac{\partial}{\partial x_j}\left(2\nu \bar{s}_{ij}\right) - \frac{\partial}{\partial x_j}\left(\overline{u_i' u_j'}\right) \tag{2}$$

$$\frac{\partial \bar{c}}{\partial t} + \frac{\partial}{\partial x_j}\left(\bar{c}\bar{u}_j\right) = \frac{\partial}{\partial x_j}\left(D\frac{\partial \bar{c}}{\partial x_j}\right) - \frac{\partial}{\partial x_j}\left(\overline{c' u_j'}\right) \tag{3}$$

where $u_i$ and $x_i$ = velocity
$t$ = time
$\rho$ = density
$p$ = pressure
$\nu$ = fluid kinematic viscosity
$c$ = concentration
$s_{ij}$ = strain-rate tensor
$\left(\overline{u_i' u_j'}\right)$ and $\left(\overline{c' u_j'}\right)$ = Reynolds stress and turbulence mass

In addition, this study includes a grid independence study, comparing coarse, medium and fine meshes, and three different domains with wind angles ranging from 0˚ to 30˚ to determine the optimum environment for each simulation. This was achieved by analyzing the coarse, medium, and fine wind velocity values for each wind angle simulation. The medium meshes have been chosen for all three simulations based on this grid study. This is due to the comparable ability of the medium mesh with the fine mesh to produce a reliable wind computation, whereby the fine mesh consumes a higher computation time than the coarse mesh. The selected simulations for all three wind angles emerged in the next phase.

### 2.3 Data Analysis

The analysis phase assesses the wind velocity and pedestrian wind comfort. The wind flow pattern and analysis were thoroughly observed to describe the wind simulation environment for all different wind angles. Meanwhile, pedestrian wind comfort was assessed using the Beaufort wind force scale (BWS) (limona et al., 2019) for 0˚, 15˚, and 30˚ wind angles. Table 1 below shows the BWS for reference.

| Force | Wind speed (m/s) | Descriptive Terms |
|---|---|---|
| 0 | <0.3 | Calm |
| 1 | 0.3 to 1.5 | Light air |
| 2 | 1.6 to 3.3 | Light breeze |
| 3 | 3.4 to 5.4 | Gentle breeze |
| 4 | 5.5 to 7.9 | Moderate breeze |
| 5 | 8.0 to 10.7 | Fresh breeze |
| 6 | 10.8 to 13.8 | Strong breeze |
| 7 | 13.9 to 17.1 | High wind |
| 8 | >17.1 | Gale |

**Table 1**. Beaufort wind force scale (BWS).

## 3. RESULTS AND DISCUSSIONS

The 3D building model to be amalgamated in the wind CFD simulation environment is represented in LoD2.3 (Figure 1). This model consists of a roof overhang structure. The existence of this structure allows for the presence of the hollow shape to enable the observation of the wind impact at that location. To observe the effect, the wind velocity from the wind simulation results of 0˚, 15˚, and 30˚ wind angle is presented in Figures 4 and 5.

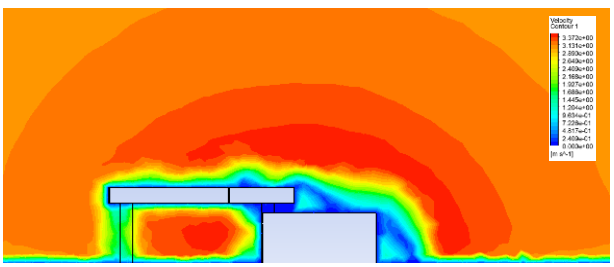

(a)

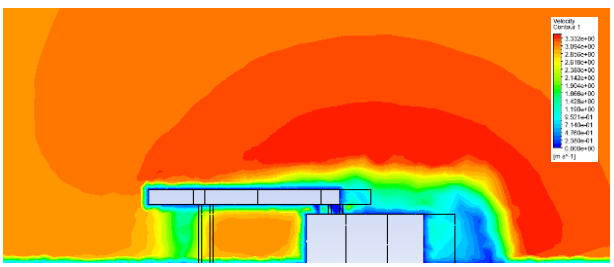

(b)

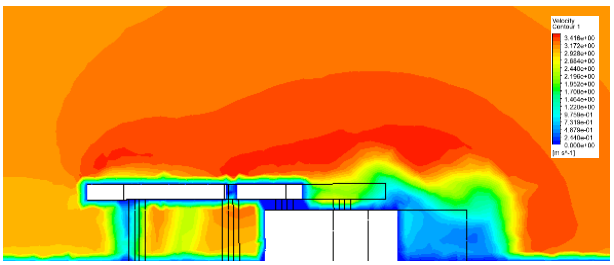

(c)

**Figure 4.** Wind CFD simulation result of different wind angles from side perspectives. (a) 0˚, (b) 15˚, and (c) 30˚.

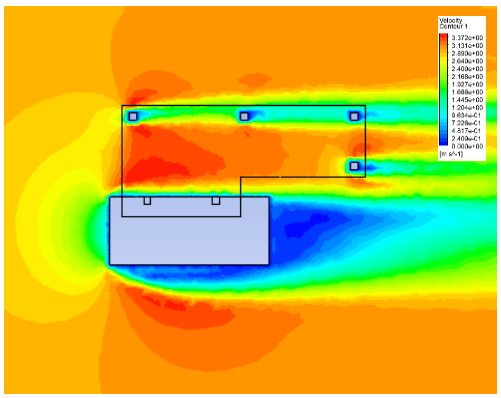

(a)

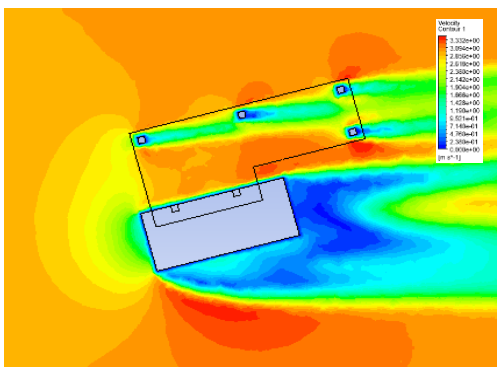

(b)

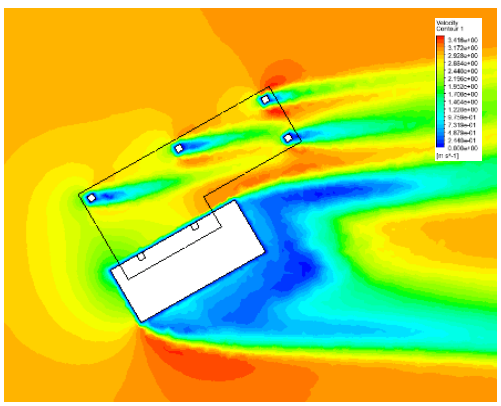

(c)

**Figure 5.** Wind CFD simulation result of different wind angles from top perspectives. (a) 0˚, (b) 15˚, and (c) 30˚.

The medium mesh size is chosen as the optimal environment for simulating three different wind angles because of its ability to achieve stable parameter values without using more computational time. Additionally, the findings are displayed using the x and z planes to display the various simulation results. Figures 4(a), (b), and (c) and 5(a), (b) and (c) depict the difference in the wind velocity contours. The results are influenced by the wind flow pattern. According to Kheyari & Dalui (2015), the basic idea behind the wind flow pattern is that the wind will separate as it hits the building model. However, the separations are varied. The blue colour in the simulation result represents the formation of low wind velocity. Wind flow will deviate from the building model due to flow separation by moving to both of the building's vertical edges, above and downward (Kasana et al., 2022; Rajasekarababu et al., 2019).

As a result, the leeward side is not directly supplied with wind. Consequently, the wind speed downstream of the structure will be lower than the wind speed coming in, especially near the building. The building, a solid item without porosity traits that may allow the wind to flow through, also supports the slowing impact of the wind velocity. However, because the wind flow will reach the wake zone to restore the wind velocity, this situation only happens at close range. Furthermore, due to the flow separation, the wind recirculation around the building model can also occur on the leeward and windward sides (Ozmen et al., 2016). However, the leeward side exhibits a more notable recirculation. Due to the backward flow and surrounding pressure close to the building model, recirculation occurs. This event produces a low wind velocity as a result of the wind slowdown during the flow separation occurrence.

In addition, the wake zone, indicated by the cyan colour, can also convey the flow pattern. According to Sattar et al., (2018), the wake region distance often falls within a narrow range of the building height. This area is located following the downstream recirculation area of the building. This sector, which is the continuation of the recirculation area, recovers wind speed from the flow separation process from the windward side, where the flow re-attaches to produce increased wind speed. The zone with the highest wind velocity value after the wake region is the flow, which is depicted by the green colour. Because there is less obstacle that can potentially create greater flow separation from other parts, momentum is regained. The flow of this area continues to provide the degree of separation from the wake region. The area without obstacles where the flow can have roughly the same velocity as the input or incoming velocity is typically connected with the flow pattern represented by the yellow colour range.

Moreover, when the flow glides over the structure at the top of the building, the wind pattern that produces the flow separation from the windward side occurs, causing a variation in wind speed (Moonen et al., 2012; Tasneem et al., 2020). Variation enables the incoming wind to influence the wind speed with slightly higher and lower values. The interaction of the wind near the building's corner causes the highest wind velocity to be represented. The building upstream experiences a significant amount of wind flow that goes downward due to the incoming wind that diverges around and over the structure. According to van Druenen et al., (2019), the downward movement creates a standing vortex that will continue to swirl around the building corner and form a high-speed wind corner stream.

Furthermore, the result also depicts the difference in the computed wind velocity from the three directions of wind angles. With the observation subjected to the area beneath the roof overhang, the wind velocity produced from 0˚ wind angles has the highest values compared to the simulation domain of 15˚ and 30˚ angles. This is because the 0˚ incoming wind flow is not obstructed by any structure from the wind inlet. Therefore, there is a parallel wind flow that results in high wind velocity. The lower values of wind velocity in the 15˚ and 30˚ situations may be due to the wind being blocked by the building structure, causing flow separation and reducing wind velocity.

For the assessment of pedestrian wind comfort, wind velocity values at multiple locations with 1.75m height are recorded in Figure 6 for the three wind angles. Based on this figure, 0˚ angle presents the highest value of 3.476 m/s, followed by 15˚ with 3.21 m/s and 30˚ with 2.702 m/s. However, the highest values cannot reflect the actual state of the study area. Hence, from all recorded values, the average wind speed that the pedestrian can encounter is collected, where 3.24 m/s corresponds to a wind angle of 0°, 2.761 m/s for 15˚, and 2.415 m/s for 30˚. Using the average value as a reference to compare with the wind comfort criteria, all these average values fall in scale level 2, which specifies that the area experiences a light breeze and the pedestrian will feel the wind on exposed skin. Nonetheless, the most tranquil surrounding comes from the 30˚ wind angle due to the lowest wind velocity value.

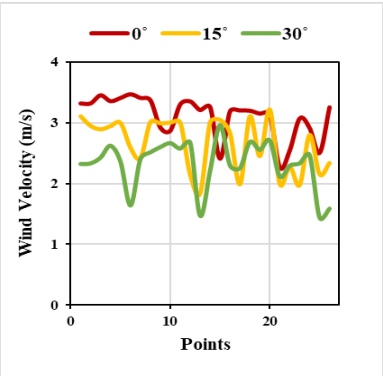


**Figure 6**. Wind velocity recorded for pedestrian wind comfort analysis.

## 4. CONCLUSION

This study observes the influence of wind flow under the existence of roof overhang structures and its relation to pedestrian wind comfort. The study was carried out by implementing the LoD2.3 standalone building model to represent the building with a specific structure: roof overhang. The embedding of LoD, which is of city modelling standard, allows the building representation with optimum representation in a wind CFD environment. The process of simulating the wind environment with the integration of this LoD2.3 model used steady RANS with k-Ɛ turbulence model to represent incompressible wind flow.

Different wind angles of 0˚, 15˚, and 30˚ angles have been included to study further the wind impact on the model. From the observation, all of these three wind angles result in distinct wind flow and velocity. This is due to the wind that comes from different directions and interacts with varying design surfaces or the building structure. Furthermore, it is also affected by the existence of the roof overhang structure. The observed area beneath the roof overhang structure has the highest wind velocity value in the 0˚ wind angle, continuing by 15˚ and 30˚ wind angles. This is because the 0˚ domain introduces an area

without obstruction, allowing fast-moving wind to travel beneath the roof overhang. Furthermore, in analysing the pedestrian wind comfort of these areas affected by different wind angles, wind velocity at multiples point locations have been recorded, and the outcomes through the computed average values show that 3.24 m/s corresponds to a wind angle of 0°, 2.761 m/s for 15˚, and 2.415 m/s for 30˚. Through this result, all the values fall in the BWS of scale 2, which indicates the ability to experience a light breeze. However, the lowest velocity value from 30˚ wind angle- simulation environment gives the most tranquil environment.

## ACKNOWLEDGEMENTS

This research was funded by UTM Research University Grant, Vot Q.J130000.2452.09G84.

## REFERENCES

Azri, S., Ujang, U., Abdul Rahman, A., 2018. Dendrogram clustering for 3D data analytics in smart city. *International Archives of Photogrammetry, Remote Sensing and Spatial Informtion Science*, 4249(4/W9), 247–253. https://doi.org/10.5194/ISPRS-ARCHIVES-XLII-4-W9-247-2018

Azri, S., Ujang, U., Abdul Rahman, A., 2020. Voronoi classified and clustered data constellation: A new 3D data structure for geomarketing strategies. *ISPRS Journal of Photogrammetry and Remote Sensing*, 162, 1–16. https://doi.org/10.1016/J.ISPRSJPRS.2020.01.022

Franke, J., Hellsten, A., Schlünzen, K. H., Carissimo, B., 2007. Best practice guideline for the CFD simulation of flows in the urban environment-a summary. *11th Conference on Harmonisation within Atmospheric Dispersion Modelling for Regulatory Purposes*. UK: Cambridge Environmental Research Consultants

García-Sánchez, C., Vitalis, S., Paden, I., Stoter, J., 2021. The impact of level of detail in 3D city models for CFD-based wind flow simulations. *Int. Arch. Photogramm. Remote Sens. Spatial Inf. Sci.*, XLVI-4/W4-, 67–72

Hågbo, T.-O., Giljarhus, K. E. T., Hjertager, B. H., 2021. Influence of geometry acquisition method on pedestrian wind simulations. *Journal of Wind Engineering and Industrial Aerodynamics*, 215, 104665. https://doi.org/https://doi.org/10.1016/j.jweia.2021.104665

Kasana, D., Tayal, D., Choudhary, D., Raj, R., Meena, R. K., Anbukumar, S., 2022. Evaluation of aerodynamic effects on a tall building with various cross-section shapes having equal area. *Forces in Mechanics*, 9, 100134. https://doi.org/https://doi.org/10.1016/j.finmec.2022.100134

Kaseb, Z., Hafezi, M., Tahbaz, M., Delfani, S., 2020. A framework for pedestrian-level wind conditions improvement in urban areas: CFD simulation and optimization. *Building and Environment*, 184, 107191. https://doi.org/10.1016/J.BUILDENV.2020.107191

Kheyari, P., Dalui, S. K., 2015. Estimation of wind load on a tall building under interference effects : A case study. *Jordan Journal of Civil Engineering*, 2015 9(1), 84–101, 1–18.

limona, S. S., Al-hagla, K. S., El-sayad, Z. T., 2019. Using simulation methods to investigate the impact of urban form on human comfort. Case study: Coast of Baltim, North Coast, Egypt. *Alexandria Engineering Journal*, 58(1), 273–282. https://doi.org/https://doi.org/10.1016/j.aej.2019.02.002

Mohd, Z. H., Ujang, U., Choon, T. L., 2017. Heritage house maintenance using 3D city model application domain extension approach. *International Archives of the Photogrammetry, Remote Sensing and Spatial Information Sciences - ISPRS Archives*, 42(4W6), 73–76. https://doi.org/10.5194/ISPRS-ARCHIVES-XLII-4-W6-73-2017

Moonen, P., Defraeye, T., Dorer, V., Blocken, B., Carmeliet, J., 2012. Urban Physics: Effect of the micro-climate on comfort, health and energy demand. *Frontiers of Architectural Research*, 1(3), 197–228. https://doi.org/10.1016/J.FOAR.2012.05.002

Ozmen, Y., Baydar, E., van Beeck, J. P. A. J., 2016. Wind flow over the low-rise building models with gabled roofs having different pitch angles. *Building and Environment*, 95, 63–74. https://doi.org/https://doi.org/10.1016/j.buildenv.2015.09.014

Rajasekarababu, K. B., Vinayagamurthy, G., Selvi Rajan, S., 2019. Experimental and computational investigation of outdoor wind flow around a setback building. *Building Simulation*, 12(5), 891–904. https://doi.org/10.1007/S12273-019-0514-8/METRICS

Ridzuan, N., Ujang, U., 2021. Determination of suitable level of details (LoD) Of 3D building model for air pollutants dispersion study. *6th Geoinformation Research Colloquium, Morocco*.

Ridzuan, N., Ujang, U., Azri, S., Choon, T. L., 2020. Visualising urban air quality using AERMOD, CALPUFF and CFD models: A critical review. *International Archives of the Photogrammetry, Remote Sensing and Spatial Information Sciences - ISPRS Archives*, 44(4/W3), 355–363. https://doi.org/10.5194/isprs-archives-XLIV-4-W3-2020-355-2020

Salleh, S., Ujang, U., Azri, S., 2021. Virtual 3D Campus for Universiti Teknologi Malaysia (UTM). *ISPRS International Journal of Geo-Information 2021*, Vol. 10, Page 356, 10(6), 356. https://doi.org/10.3390/IJGI10060356

Sattar, A. M. A., Elhakeem, M., Gerges, B. N., Gharabaghi, B., Gultepe, I., 2018. Wind-induced air-flow patterns in an urban setting: Observations and numerical modeling. *Pure and Applied Geophysics*, 175(8), 3051–3068. https://doi.org/10.1007/S00024-018-1846-5

Singh, J., Roy, A. K., 2019. Effects of roof slope and wind direction on wind pressure distribution on the roof of a square plan pyramidal low-rise building using CFD simulation. *International Journal of Advanced Structural Engineering*, 11(2), 231–254. https://doi.org/10.1007/S40091-019-0227-3/FIGURES/20

Tasneem, Z., Al Noman, A., Das, S. K., Saha, D. K., Islam, M. R., Ali, M. F., R Badal, M. F., Ahamed, M. H., Moyeen, S. I., Alam, F., 2020. An analytical review on the evaluation of wind resource and wind turbine for urban application: Prospect and challenges. *Developments in the Built Environment*, 4. https://doi.org/10.1016/J.DIBE.2020.100033

Ujang, U., Anton, F., Suhaibah, A., Rahman, A. A., Mioc, D., 2013. Improving 3D spatial queries search: Newfangled technique of space filling curves in 3D city modeling. *ISPRS Annals of the Photogrammetry, Remote Sensing and Spatial Information Sciences*, 2(2W1), 319–327. https://doi.org/10.5194/isprsannals-II-2-W1-319-2013

Ujang, U., Azri, S., Zahir, M., Abdul Rahman, A., Choon, T. L., 2018. Urban heat island micro-mapping via 3D city model. *International Archives of the Photogrammetry, Remote Sensing and Spatial Information Sciences - ISPRS*

*Archives*, 42(4/W10), 201–207. https://doi.org/10.5194/isprs-archives-XLII-4-W10-201-2018

van Druenen, T., van Hooff, T., Montazeri, H., Blocken, B., 2019. CFD evaluation of building geometry modifications to reduce pedestrian-level wind speed. *Building and Environment*, 163, 106293. https://doi.org/10.1016/j.buildenv.2019.106293